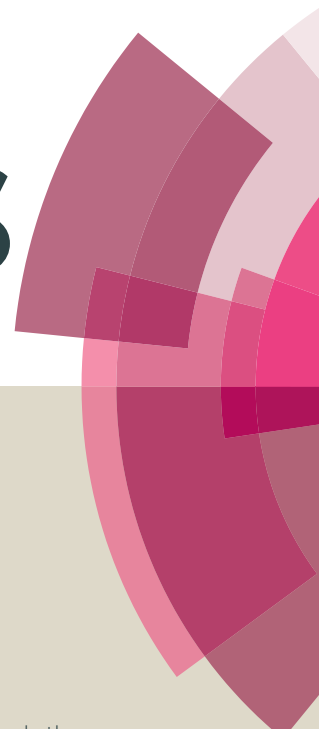


# RSC Advances



This article can be cited before page numbers have been issued, to do this please use: S. Gupta, M. I. Alam, T. S. Khan, N. Sinha and M. A. Haider, *RSC Adv.*, 2016, DOI: 10.1039/C6RA11697C.



This is an *Accepted Manuscript*, which has been through the Royal Society of Chemistry peer review process and has been accepted for publication.

*Accepted Manuscripts* are published online shortly after acceptance, before technical editing, formatting and proof reading. Using this free service, authors can make their results available to the community, in citable form, before we publish the edited article. This *Accepted Manuscript* will be replaced by the edited, formatted and paginated article as soon as this is available.

You can find more information about *Accepted Manuscripts* in the [Information for Authors](#).

Please note that technical editing may introduce minor changes to the text and/or graphics, which may alter content. The journal's standard [Terms & Conditions](#) and the [Ethical guidelines](#) still apply. In no event shall the Royal Society of Chemistry be held responsible for any errors or omissions in this *Accepted Manuscript* or any consequences arising from the use of any information it contains.

## On the Mechanism of Retro-Diels-Alder Reaction of Partially Saturated 2-Pyrones to Produce Biorenewable Chemicals

Shelaka Gupta<sup>a</sup>, Md. Imteyaz Alam<sup>a</sup>, Tuhin Suvra Khan<sup>a</sup>, Nishant Sinha<sup>b</sup>, M. Ali Haider<sup>a\*</sup>

<sup>a</sup> Renewable Energy and Chemicals Laboratory, Department of Chemical Engineering,

Indian Institute of Technology Delhi, Hauz Khas, New Delhi-110016

<sup>b</sup>Dassault Systemes, Galleria Commercial Tower, 23 Old Airport Road, Bangalore 560008

\* Corresponding author:

Tel: +91-11-26591016, Fax: +91-11-2658-2037

E-mail: haider@iitd.ac.in

### ABSTRACT:

Partially saturated 2-pyrone molecules undergo ring-opening and decarboxylation via retro-Diels-Alder (rDA) reaction. Density functional theory (DFT) simulations were utilized to calculate the intrinsic activation barrier and reaction energies of the steps involved in rDA reaction of biomass-derived 5,6-dihydro-4-hydroxy-6-methylpyran-2-one (5DHHMP), 4-hydroxy-3,6-dimethyl-pyran-2-one (4HDMP) and 4-hydroxy-6-(2oxo-propyl)-3,6-dihydro-pyran-2-one (4HOPP). The rDA reaction of the three molecules in water proceeds in two steps via the formation of a zwitterionic intermediate. The calculated activation barrier ( $E_a = 61$  kJ/mol) for the rDA reaction of 5DHHMP in water compares well with the experimentally measured value. In the absence of hydrogen bonding interactions such as in the solvent n-hexane and gas-phase, the rDA reaction is concerted and activation barriers of the three molecules were estimated to be relatively higher. Substituents at C<sub>6</sub>, C<sub>4</sub> and C<sub>3</sub> position in partially saturated 2-pyrones showed a clear effect on the reactivity of the molecules which was correlated back to the resultant normal electron demand frontier molecular orbital (FMO) gap of the product diene and dienophile. The electronic and geometric (steric) effects of the substituents were separated by including several other structurally similar molecules having variations in the position, type and number of substituents. In general, the electronic effect of the substituents follow a linear trend, where FMO gap for normal electron demand serves as a good descriptor of the reactivity. The geometric effect was represented on a linear scale to quantify the steric hindrance offered by the methyl substituents. Molecules having no hydroxyl substituent at C<sub>4</sub> such as 6-methyl-3,6-dihydro-2H-pyran-2-one (4HMTHP) and 4,6,6-trimethyl-3,6-dihydro-2H-pyran-2-one (DTMP) showed a concerted route for rDA reaction in water without the formation of the intermediate.

The rates of rDA reaction of the molecules were observed to be accelerated in water as compared to n-hexane. In solvents, the reactivity of the molecule doesn't correlate to the FMO gap of the products, likely due to the differential stabilization of the reactant and transition state. In general, polar solvents (water, DMSO, ethanol and methanol) were calculated to show lesser activation energy despite of a greater FMO gap as compared to non-polar solvents (n-hexane). In a solvent, the rDA reaction of the molecules follows a Brønsted–Evans–Polanyi (BEP) relationship. In presence of a Brønsted acid catalyst the rDA reaction of 5DHHMP proceeds via the formation of an oxocarbenium ion which further helps in facilitating the reaction with a significantly reduced activation barrier ( $E_a = 15$  kJ/mol).

### Key words

*Density functional theory, 2-pyrone, ring-opening, retro-Diels-Alder reaction, biorenewable chemicals.*

## 1. INTRODUCTION

Biomass derived platform molecules such as furans and lactones are potential feedstock to produce chemicals and fuels<sup>1–6</sup>. Strategies for catalytic transformation of these molecules include an overall deoxygenation process via a combination of reaction steps which may comprise of hydrogenolysis<sup>7,8</sup>, dehydration<sup>9</sup>, decarbonylation, ring-opening and decarboxylation<sup>10,11</sup>. Out of which ring-opening reaction followed by decarboxylation has received considerable attention, as it forms a direct step for producing the desired product. Dumesic and co-workers have experimented with a variety of solid acid catalysts for producing isomers of butene by ring-opening and decarboxylation of  $\gamma$ -valerolactone (GVL) at high temperature (>548 K) and pressure (~36 bar) conditions<sup>12</sup>. In contrast, experiments on partially saturated 2-pyrones such as 3,6-dihydro-4-hydroxy-6-methylpyran-2-one (DHHMP) have shown unprecedented activity for ring-opening and decarboxylation at mild condition (T=373 K) without the requirement of an acid catalyst. Simulations utilizing density functional theory (DFT) calculations have attributed the experimentally observed high reactivity of DHHMP to the formation of a double bond at a unique position (between C<sub>4</sub> and C<sub>5</sub>, Figure 1) in the ring via keto-enol tautomerization (KET). The resultant isomer 5,6 dihydro-4-hydroxy-6-methylpyran-2-one (5DHHMP) is suggested to ring-open and decarboxylate by a two-step retro-Diels-Alder (rDA) reaction in aqueous phase in

which  $\text{CO}_2$  is released as the product dienophile. The rDA reaction explains the high reactivity of DHHMP for ring-opening and decarboxylation without the requirement of an acid catalyst<sup>11</sup>.

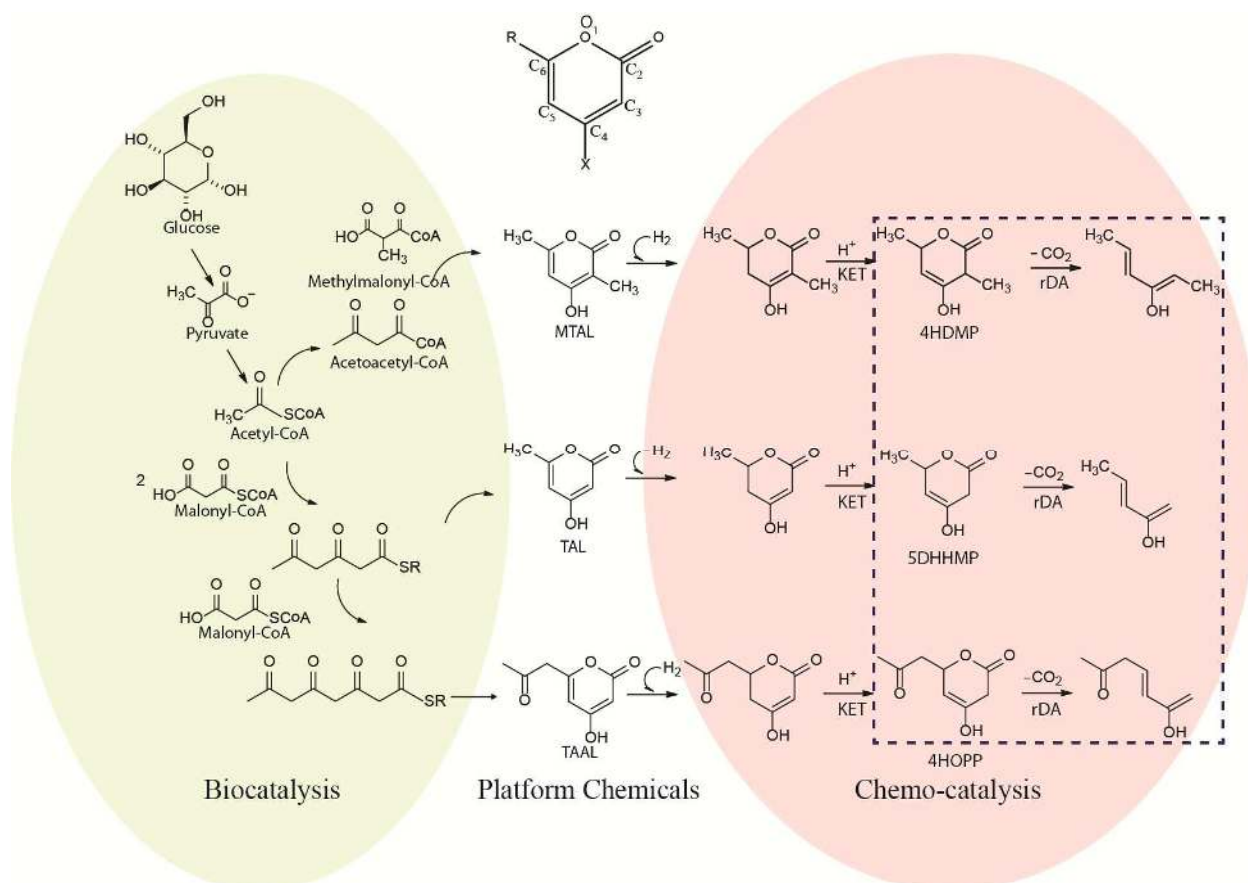


**Figure 1.** Routes for biosynthesis of selected 2-pyrone molecules and strategy for their catalytic transformation via rDA reaction. The reactions in the rectangular box is the focus of this study.

Polyketide synthesis routes in microorganisms have been suggested to produce a variety of pyrone molecules from the fermentation of biomass<sup>13–15</sup>. Microorganisms can be genetically engineered by utilizing informations from metabolic engineering to selectively produce a desired product. For example, on overexpressing *2-pyrone synthase* gene in *Saccharomyces cerevisiae*, production of triacetic acid lactone (TAL) has been reported to increase by 37 fold to a titer of 2.2 g/l in glucose fermentation<sup>16</sup>. Further catalytic upgrading can be achieved by employing a suitable heterogeneous or a homogeneous catalyst which may give the desired yield to a useful product. Substituents at the 2-pyrone molecule have shown significant effect on the reactivity in catalytic transformations<sup>11</sup>. For example, in TAL high reactivity for the ring-opening and decarboxylation reaction was attributed to the presence of a hydroxyl group at C<sub>4</sub> which leads to

the KET. Similarly, number of methyl substituents at C<sub>6</sub> were observed to significantly effect the activation barriers and consequently its reactivity via the rDA reaction<sup>11</sup>.

Variations in substituents of 2-pyrones can be biologically synthesized from the fermentation of biomass or biomass derived aqueous sugars<sup>17</sup>. Methyl triacetic acid lactone (MTAL), having a methyl substituent at C<sub>3</sub> is biologically produced from the fermentation of glucose by *Penicillium stipitatum* in which the starter unit, acetoacetyl-CoA, reacts with the extender methyl malonyl-CoA, to yield MTAL<sup>18</sup>. Similarly, tetra-acetic acid lactone (TAAL) is produced from the same metabolic route of TAL. TAAL is formed by the reaction of 2 moles of extender malonyl-CoA with the starter acetyl-CoA<sup>19</sup>. The metabolic routes for the biological synthesis of TAL, MTAL and TAAL are shown in Figure 1. The three molecules were isolated together from the strain of *Penicillium stipitatum*<sup>20,21</sup>. TAL on partial hydrogenation produces DHHMP, Figure 1. Similar to TAL, a catalytic processing route for MTAL and TAAL may involve partial hydrogenation combined with KET to produce 4-hydroxy-3,6-dimethyl-pyran-2-one (4HDMP) and 4-hydroxy-6-(2oxo-propyl)-3,6-dihydro-pyran-2-one (4HOPP) respectively as shown in Figure 1. The products thus obtained are likely to ring-open and decarboxylate via rDA reaction into hydrocarbons and ketonic molecules which can be directly or indirectly be used as a chemical or fuel additive.

The rDA reaction could proceed under moderate conditions (T=348 K) in the presence of a solvent with or without the requirement of an acid catalyst<sup>11</sup>. In general, the rDA reaction was observed to be accelerated in a polar solvent (e.g. water) as compared to a non-polar solvent (e.g. n-hexane)<sup>22</sup>. The mechanism of the rDA reaction could either be concerted or involve a stable intermediate depending upon the polarity of the solvent<sup>23</sup>. Water is suggested to affect the reactivity by stabilizing the polarized activated complex of the transition state formed during the reaction by hydrogen bonding interactions<sup>22</sup>. Furthermore, compared to a protic solvent, acid-catalyzed reaction in an aprotic solvent, in general, could lead to a greater degree of stabilization of the reactant state (relative to the transition state) which may in-turn show significant effect on measured reaction rates<sup>24</sup>. Under normal electron demand, the electron donating substituent on diene and electron withdrawing substituent on dienophile accelerates the Diels Alder (DA) reaction<sup>25,26</sup>. For example in the rDA reaction of anthracene, cycloadducts are influenced by the type of substituent on both diene and dienophile. Electron donating group on dienes were

observed to increase the reaction rate while on dienophile the same type of groups reduces the reaction rate<sup>27</sup>.

Herein the mechanism of the rDA reaction of 5DHHMP, 4HDMP and 4HOPP is studied in detail in gas-phase, polar and non-polar solvents by DFT simulations. The products (Figure 1) obtained via rDA reaction from the aforementioned partially saturated 2-pyrone molecules can be used as precursors to higher value chemicals and fuel additives. Several other model compounds were included thoughtfully to separate the geometric and electronic effects of substituent in determining the activation energies of rDA reaction. The mechanistic insights on the rDA reaction, thus explain the effect of substituents and solvents on the reactivity of the studied molecules. A linear Brønsted-Evans-Polanyi<sup>28,29</sup> (BEP) plot was envisaged to correlate reaction and activation energies of rDA reactions.

## 2. METHODS

DFT calculations with DNP (Double Numerical plus Polarization) numerical basis set were performed using the DMol<sup>3</sup> module available in Material Studio 8 (Biovia, San Diego, USA)<sup>30</sup>. Generalized gradient approximation (GGA) with Perdew and Wang's (PW91) functional was applied to describe the exchange correlation energy and potential<sup>31</sup>. For geometry optimization and transition state search, DMol<sup>3</sup> specified "Fine" convergence criteria for energy, force and atom displacement was set to 0.0001 eV, 0.05 eV/ Å and 0.005 Å respectively. Self-consistent field calculations of electron density were converged to  $1 \times 10^{-6}$  value with a density mixing parameter set to 0.02.

Solvent environment was simulated using conductor-like screening model (COSMO)<sup>32</sup> in which solvents were represented by their respective dielectric constant; water ( $\epsilon=78.54$ ), ethanol ( $\epsilon=24.3$ ), methanol ( $\epsilon=32.63$ ), chloroform ( $\epsilon=4.806$ ) and n-hexane ( $\epsilon=1.89$ ). The activation barriers were calculated by performing a transition state (TS) search by linear synchronous transit/quadratic synchronous transit (LST/QST) method<sup>33</sup>. Atomic charges associated with the transition state or the reactant state were calculated using the Mulliken population analysis<sup>34</sup>. In LST a set of single point calculations were performed on a set of linearly interpolated structures between reactant and product. The first estimate of TS structure is provided by the maximum energy structure along this path. Subsequently, the structure is refined in orthogonal direction to



the QST, which is further used as an intermediate for QST pathway. The method thus yields a refined transition state geometry. Transition state thus obtained is further refined with the 'TS Optimization' module in DMol<sup>3</sup>. In this technique the optimization starts with the transition state structure obtained from LST/QST method and is searched for energy maxima along a normal mode using the Newton-Raphson line search algorithm. All the transition states obtained in this study were verified using vibrational frequency analysis confirming presence of a single imaginary frequency vibrational mode along the reaction coordinate. The LST/QST method for finding transition states has been extensively used in the previous studies<sup>35,36</sup>. The dipole moment, highest occupied molecular orbital (HOMO) and lowest unoccupied molecular orbital (LUMO) of the respective structures were obtained using the properties implemented in DMol<sup>3</sup>. The reaction rate constants were calculated using 'Reaction Kinetics' tab in DMol<sup>3</sup>. Rate constants were calculated using canonical partition functions of the reactant, transition state and reaction threshold energy as follows:

$$k(\beta) = \frac{Q^*(\beta, R^*)}{\beta h Q(\beta)} e^{-\beta E_0}$$

Where:

$$\beta = \frac{1}{k_B T}$$

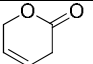
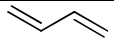
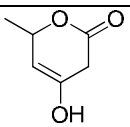
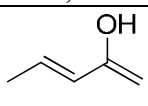
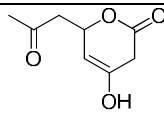
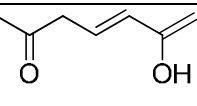
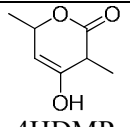
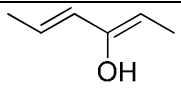
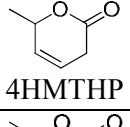
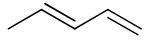
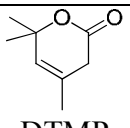
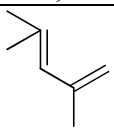
$Q^*(\beta, R^*)$  is the partition function of the transition state configuration,  $E_0$  is the threshold energy and  $Q(\beta)$  is the partition function for reactant state,  $k_B$  is the Boltzmann constant,  $T$  is the temperature and  $h$  is the Planck's constant.

### 3. RESULTS AND DISCUSSION

The reactivity of a Diels-Alder (DA) reaction in gas-phase is dictated by the frontier molecular orbital (FMO) theory involving highest occupied molecular orbital (HOMO) and lowest unoccupied molecular orbital (LUMO)<sup>37</sup>. For example in case of a normal electron demand, the energy gap between the HOMO of the diene and LUMO of the dienophile for rDA reaction could explain the reactivity<sup>27</sup>. Therefore, it can be envisaged that the FMO gap between a diene and a dienophile will influence the rate of ring-opening and decarboxylation of a 2-pyrone molecule via the rDA reaction. To begin with, for a model 2-pyrone compound 3,6-dihydro-2H-

pyran-2-one (DHHP), the FMO gap for normal electron demand was calculated to be 0.1893 Ha which was observed to be lesser than the inverse electron demand FMO gap (0.2703 Ha) (Table 1). Therefore, the rDA reaction is expected to follow the normal electron demand, which is indeed the case for all the molecules studied in this work as shown in Table 1. The model compound DHHP undergo ring-opening and decarboxylation via rDA reaction to produce CO<sub>2</sub> as the dienophile and buta-1,3-diene as the diene. The corresponding activation barrier for the concerted reaction is 136 kJ/mol (1 to TS<sub>1a</sub>, Figure S1) in the gas-phase (Figure S1).

**Table 1.** FMO gaps for normal and inverse electron demand energy gaps between the highest occupied molecular orbital of diene and lowest unoccupied molecular orbital of dienophile (CO<sub>2</sub>) of the resultant products of rDA reaction in gas-phase.

Reactant	Product	HOMO	LUMO	Normal (LUMO <sub>dienophile</sub> -HOMO <sub>diene</sub> )	Inverse (LUMO <sub>diene</sub> - HOMO <sub>dienophile</sub> )	Activation Energies (kJ/mol)
 DHHP	 buta-1,3-diene	-0.2105	-0.0656	0.1893	0.2703	136
 5DHHMP	 penta-1,3-dien-2-ol	-0.1895	-0.0548	0.1683	0.2811	94
 4HOPP	 6-hydroxyhepta-4,6-dien-2-one	-0.2001	-0.0666	0.1789	0.2923	127
 4HDMP	 hexa-2,4-dien-3-ol	-0.1793	-0.0505	0.1581	0.2854	107
 4HMTHP	 Penta-1,3-diene	-0.1982	-0.0588	0.177	0.2693	117
 DTMP	 2,4-dimethylpenta-1,3-diene	-0.1927	-0.0436	0.1715	0.2771	123



On adding a methyl substituent at C<sub>6</sub> and a hydroxyl substituent at C<sub>4</sub> to the model compound, 5DHHMP is formed, which can be derived from TAL (Figure 1). The methyl and the hydroxyl group donate the electron density to the diene thereby increasing its HOMO energy and in-turn reducing FMO gap. Indeed, the resultant FMO gap (0.1683 Ha, Table1) was observed to be lower as compared to the model compound DHHP. The reduction in the FMO gap translated into the corresponding reduction in the activation energy ( $E_a = 94$  kJ/mol, 2 to TS<sub>2a</sub><sup>\*\*</sup>) for ring-opening and decarboxylation of 5DHHMP in the gas-phase, Figure 2.

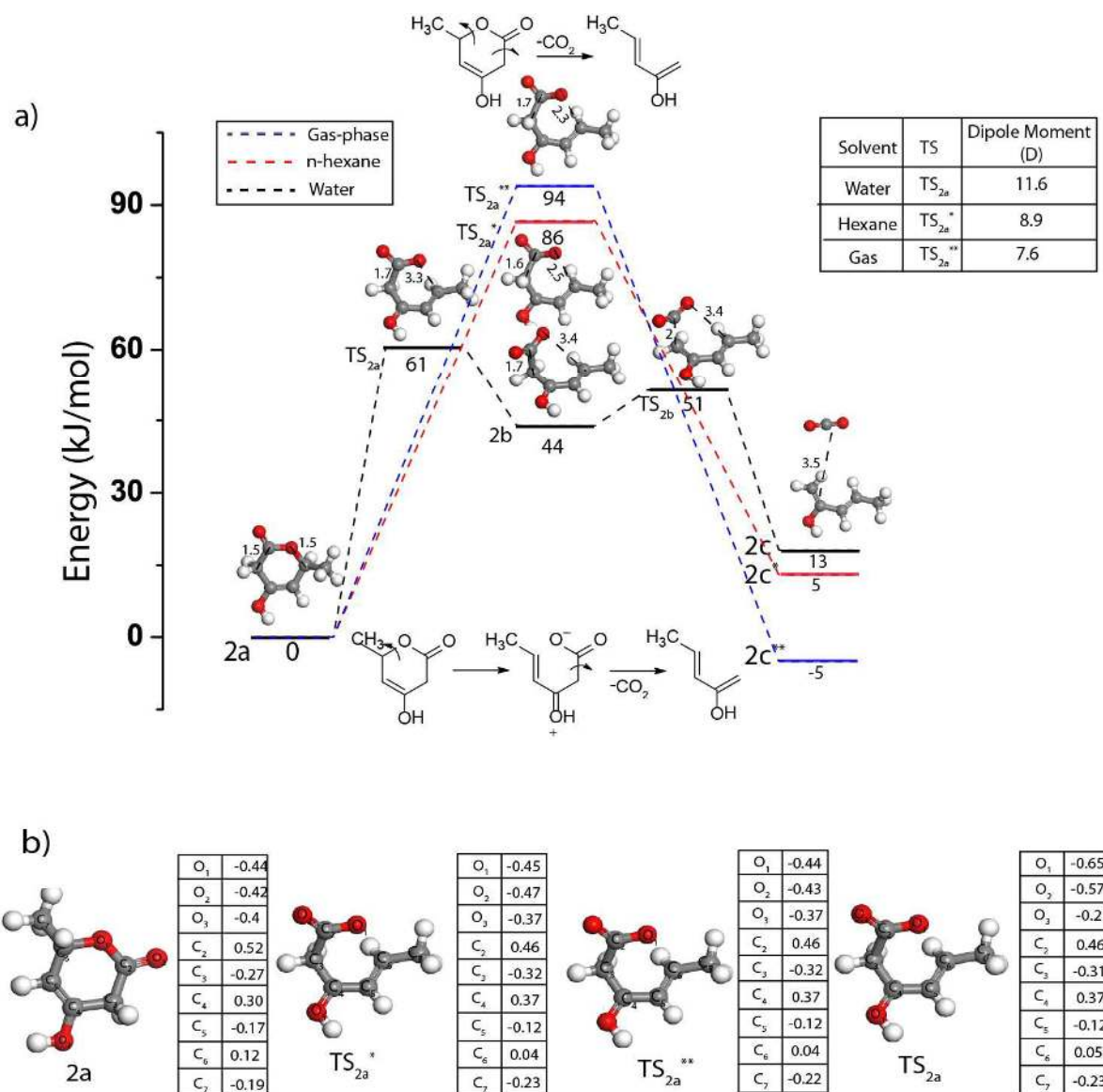


**Figure 2.** a) Reaction diagram for rDA reaction of 5DHHMP in water, n-hexane and gas-phase. b) Mulliken charge analysis for the reactant (2a) and transition states in water (TS<sub>2a</sub>\*), n-hexane (TS<sub>2a</sub>\*) and gas-phase (TS<sub>2a</sub>\*\*).

In an earlier study, DFT simulations performed by the corresponding author of this study has shown that the presence of water could lead to the stabilization of a zwitterionic intermediate by hydrogen bonding interactions, which translates into a two-step rDA reaction<sup>11</sup>, that have been explained in terms of apparent activation barrier. The apparent activation barrier for the overall reaction is calculated from the energy difference between the highest transition state and the reactant state. The apparent activation barrier for the two-step rDA reaction was observed to be lower than the concerted route. These observations were contrary to the suggested lowering of activation barrier in a concerted route as observed in rDA reaction of cyclohexene in gas-phase by a femtosecond-resolved mass spectrometry experiment<sup>38</sup>. In addition, presence of an aqueous environment may show differential hydrogen bonding interactions with the transition state and hydrophobic interaction with respect to the reactant state, which could lead to a net reduction in the activation energy<sup>39</sup>. The geometry of the reactant molecule (or the size and number of substituents in 2-pyrones) is important in this case as it may alter the solvent accessible surface area (SASA) for hydrogen bonding interactions<sup>37</sup>.

The result of the aforementioned effects translated into the reduction of the activation barrier for the ring-opening and decarboxylation of 5DHHMP in water. The intrinsic barriers for the two-step reaction were observed to be significantly reduced as compared to the concerted reaction and were calculated to be 61 kJ/mol (2a to TS<sub>2a</sub>) and 7 kJ/mol (2b to TS<sub>2b</sub>) as shown in Figure 2. The calculated value is comparable to the experimentally reported activation barrier (42±18 kJ/mol) for the ring-opening and decarboxylation of DHHMP. In a different set of experiments to study the rDA reaction of 4*H*-1,2-benzoxazines it was observed that the rate of rDA reaction and the product yield changes with varying polarity of the solvents<sup>40</sup>. For example for unsubstituted 4*H*-1,2-Benzoxazines the rDA reaction was accelerated in polar solvent such as dimethyl sulfoxide. Similar effects could be envisaged for the rDA reaction of 5DHHMP on altering the solvent. Experimental results by Chia *et al.* have shown that in absence of an acid catalyst and in similar reaction conditions, DHHMP undergo ring-opening and decarboxylation in water measuring >90% conversion and 37.1 % selectivity, while in THF the conversion was negligible (<4%)<sup>11</sup>. The high reactivity in water was attributed to the stabilization of the transition state by hydrogen bonding interaction and formation of the zwitterionic intermediate<sup>11</sup>. Similarly, in a non-polar solvent, such as n-hexane, higher activation barriers was expected and calculated to be 86 kJ/mol

(Fig. 2. 2a to  $TS_{2a}^*$ , Figure 2). The reaction proceeds via a concerted route without the formation of the zwitterionic intermediate.

Mulliken charge analysis of the transition state ( $TS_{2a}$ ,  $TS_{2a}^*$  and  $TS_{2a}^{**}$ ) of the ring-opening step in gas-phase, water and n-hexane unravels that the  $C^+-O^-$  polarization is maximum ( $C^{+0.05}-O^{-0.65}$ ) in water, while it is of similar value in n-hexane ( $C^{+0.04}-O^{-0.45}$ ) and gas-phase ( $C^{+0.04}-O^{-0.44}$ ) as shown in Figure 2 (b). Similarly, the polarization of the ring-opened activated state ( $C^{+0.05}-O^{-0.65}$ ,  $TS_{2a}$ ) is higher (Figure 2 (b)) as compared to the reactant 5DHHMP ( $C^{+0.12}-O^{-0.44}$ ) in water. The increased polarization, resulting into higher dipole moment (11.7 D), of the activated charged complex in water ( $TS_{2a}$ ) explains the bifurcation of the concerted step into a two step mechanism. As expected, the dipole moment of the activated complex in n-hexane ( $TS_{2a}^*$ , 8.93 D) and gas-phase ( $TS_{2a}^{**}$ , 7.57 D) were calculated to be relatively lower as compared to the one in water. During the progress of the reaction,  $C_2-C_3$  and  $C_6-O_1$  distance were measured in the respective transition state structures;  $TS_{2a}$ ,  $TS_{2a}^*$  and  $TS_{2a}^{**}$ . The ring-opened  $TS_{2a}$ ,  $TS_{2a}^*$  and  $TS_{2a}^{**}$  structures (Figure 2a) measure  $C_2-C_3$  bond length of 1.7 Å, which is slightly increased as compared to the reactant state (1.5 Å). In contrast, the  $C_6-O_1$  separation of the transition state structures in gas-phase, n-hexane and water were measured to be 2.3, 2.5 and 3.4 Å respectively which is significantly activated as compared to the reactant (1.5 Å). The increased separation combined with charge polarization of the transition state in water confirms to the higher values of the calculated dipole moment. The structure of the transition state in water ( $TS_{2a}$ ) is similar to the zwitterionic intermediate (2b), indicating the bifurcation to two-step rDA reaction. Whereas the ring-opened transition states in n-hexane ( $TS_{2a}^*$ ) and gas-phase ( $TS_{2a}^{**}$ ) are reactant like suggesting towards a concerted route of rDA reaction. The rDA reaction of 5DHHMP is in thermal equilibrium which is similar to calculations reported in previous study<sup>11</sup>. However, differential hydrogen bonding interactions of the reactant molecule versus the product molecule are expected to change the reaction energetics<sup>39</sup>. The effect could be more pronounced in polar solvent such as in water as compared to the non-polar solvent, n-hexane. Thus, the reaction energy for the rDA reaction of 5DHHMP in water and n-hexane were calculated to be 13 and 5 kJ/mol respectively, Figure 2.

In order to understand the effect of substituent at C<sub>6</sub> on the rDA reaction of 2-pyrone, an additional biomass-derived 2-pyrone molecule (4HOPP) was included in this study. 4HOPP contains a carbonyl substituent at C<sub>6</sub> (-CH<sub>2</sub>COCH<sub>3</sub>) which is an electron withdrawing substituent. Compared to 5DHHMP, the keto substituent in 4HOPP is expected to withdraw electrons from the diene, thereby lowering its HOMO and thus increasing the FMO gap. Indeed, the FMO gap was calculated to be 0.1789 hartree (Table 1), which was observed to be greater than 5DHHMP and the model compound DHHP. Consequently, a higher activation barrier ( $E_a=125$  kJ/mol) for the ring-opening and decarboxylation of 4HOPP in gas-phase was calculated as shown in Figure 3 (4 to TS<sub>4</sub><sup>\*\*</sup>).

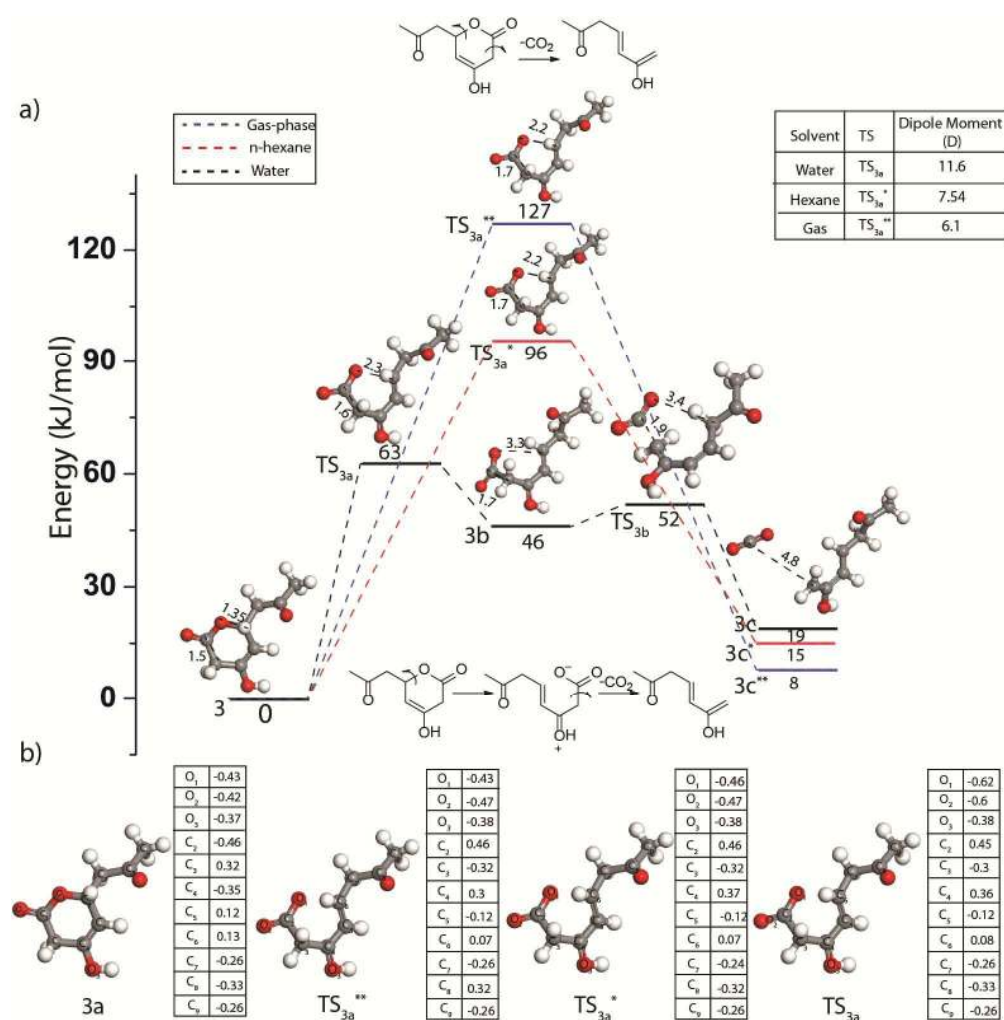


**Figure 3.** a) Reaction diagram for rDA reaction of 4HOPP in water, n-hexane and gas-phase. b) Mulliken charge analysis for the reactant (3a) and transition states in water (TS<sub>3a</sub>), n-hexane (TS<sub>3a</sub><sup>\*</sup>) and gas-phase (TS<sub>3a</sub><sup>\*\*</sup>).

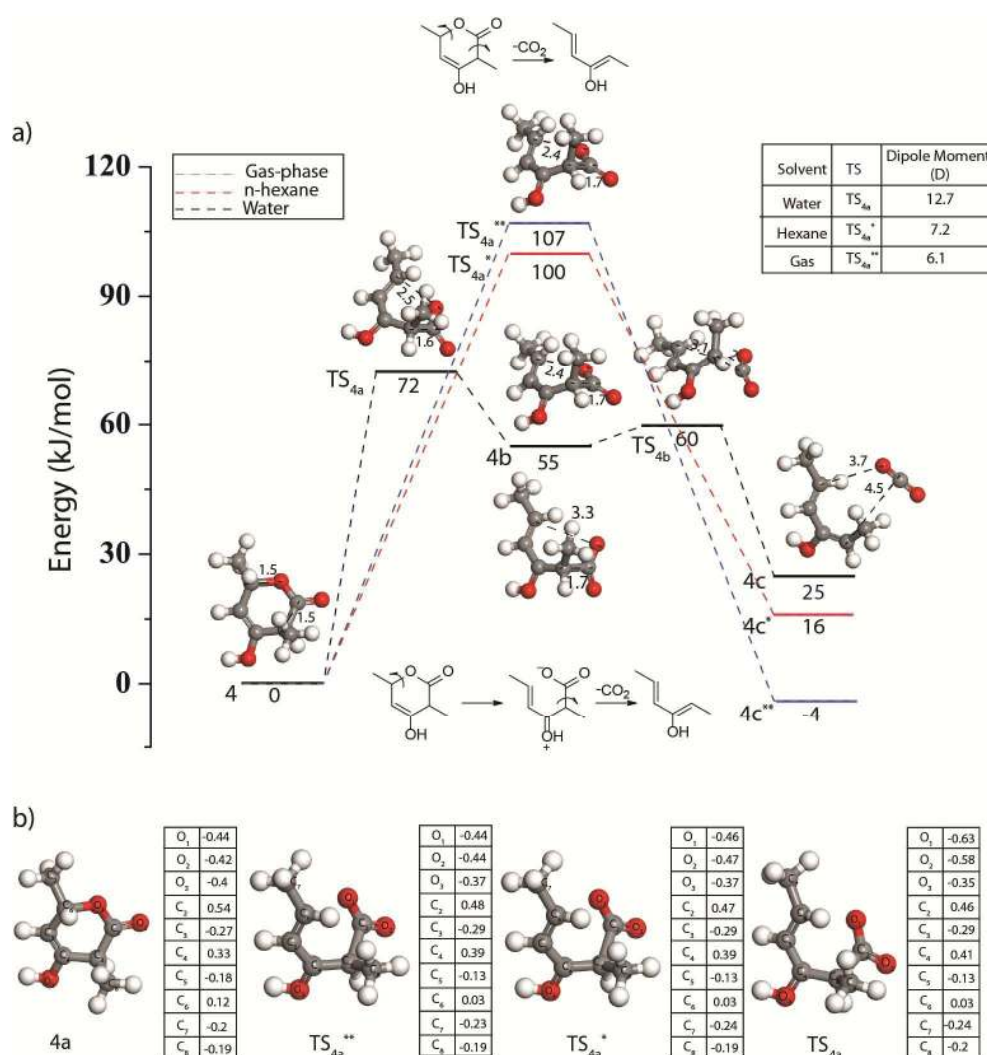
The resultant product 6-hydroxyhepta-4,6-dien-2-one is used as a precursor for the production of other chemicals<sup>41</sup>. Similar to 5DHHMP, 4HOPP tends to ring-open and decarboxylate by forming a zwitterionic intermediate in water with a reduced activation barrier of 63 kJ/mol (3a to TS<sub>3a</sub>), which is comparable to the activation barrier of 5DHHMP (61 kJ/mol) in water. Increased FMO gap for 4HOPP (0.1826 Ha) compared to 5DHHMP (0.1772 Ha) in water did not result in higher activation barrier, as observed for gas-phase reaction. The FMO gap can only be used to explain rDA reaction in gas-phase, and has been found to be inadequate to explain reactivity in solvents<sup>42</sup>.

While in n-hexane, rDA reaction occurs via the concerted step with a relatively higher activation energy of 96 kJ/mol (3a to TS<sub>3a</sub><sup>\*</sup>). The C<sub>2</sub>-C<sub>3</sub> bond length was measured to be the same in the reactant and transition states structures (Figure 3), indicating that the ring-opening occurs before the decarboxylation is started. The C<sub>6</sub>-O<sub>1</sub> separation was increased from 1.35 Å (Figure 3 (3a)) to approximately 2.2 Å in the respective transition states in gas-phase, n-hexane and water. While the C<sub>6</sub>-O<sub>1</sub> separation remains the same for TS<sub>3a</sub>, TS<sub>3a</sub><sup>\*</sup> and TS<sub>3a</sub><sup>\*\*</sup>, charge polarization (C<sup>+0.08</sup>-O<sup>-0.62</sup>) for TS<sub>3a</sub> was measured to be higher as compared to TS<sub>3a</sub><sup>\*</sup> (C<sup>+0.07</sup>-O<sup>-0.46</sup>) and TS<sub>3a</sub><sup>\*\*</sup> (C<sup>+0.07</sup>-O<sup>-0.43</sup>). Consequently, the dipole moment of TS<sub>3a</sub> (11.51 D) was estimated higher than TS<sub>3a</sub><sup>\*</sup> (7.54 D) and TS<sub>3a</sub><sup>\*\*</sup> (6.1 D), indicating greater polarization of TS<sub>3a</sub> in water. The intrinsic activation energy for the decarboxylation of the resultant zwitterionic intermediate was calculated to be 6 kJ/mol which is the same as observed in the decarboxylation of 5DHHMP. Thus, decarboxylation in water via the activation of the C<sub>2</sub>-C<sub>3</sub> bond remains unaffected by the change in substituent at C<sub>6</sub>.

A methyl substituent at C<sub>3</sub> could possibly have more influence on the C<sub>2</sub>-C<sub>3</sub> bond activation, as well as the ring-opening step. To study this hypothesis, 4-hydroxy-3,6-dimethyl-3,6-dihydro-2H-pyran-2-one(4HDMP) was included for DFT simulations. On ring-opening, decarboxylation and KET reactions, 4HDMP produces hex-4-en-3-one which is used as a flavoring agent<sup>43</sup>. Similar to DHHMP and 4HOPP, 4HDMP ring-opens first via forming a stable zwitterion ion in water as shown in Figure 4 (4 to 4a), with an activation barrier of 72 kJ/mol which subsequently decarboxylates to hexa-2,4-dien-3-ol. The activation barrier in water was considerably reduced, compared to the value of E<sub>a</sub> =107 kJ/mol for concerted reaction in gas-phase (Figure 4, 4 to



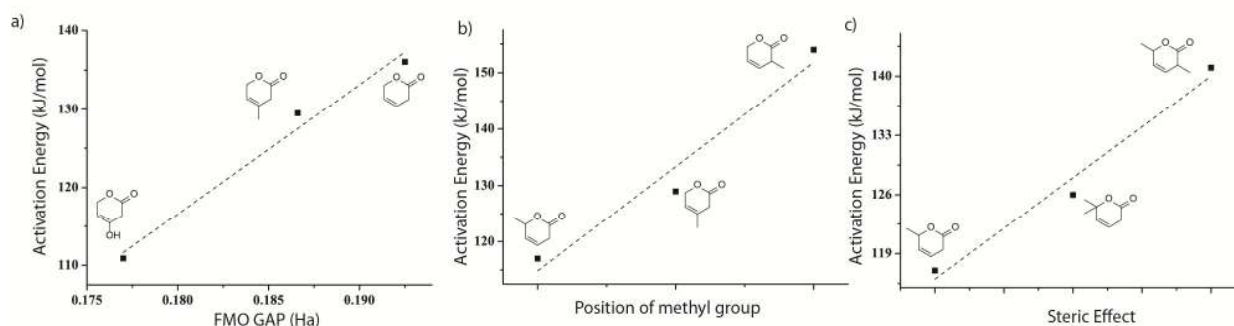
TS<sub>4a</sub><sup>\*\*</sup>). Similarly, absence of hydrogen bonding interaction in n-hexane led to a higher estimate of E<sub>a</sub>=100 kJ/mol (Figure 4, 4 to TS<sub>4a</sub><sup>\*</sup>). The transition states in water (TS<sub>4a</sub>), n-hexane (TS<sub>4a</sub><sup>\*</sup>) and gas-phase (TS<sub>4</sub><sup>\*\*</sup>) show a ring-opened structure C<sub>6</sub>-O<sub>1</sub> bond separation of 2.5 Å, 2.4 Å and 2.4 Å respectively. Mulliken charge analysis on the ring-opened structures show that the charge separation for TS<sub>4a</sub> (C<sup>+0.03</sup>-O<sup>-0.63</sup>) is higher, and hence is more polarized compared to the one obtained in n-hexane (TS<sub>4a</sub><sup>\*</sup>, C<sup>+0.03</sup>-O<sup>-0.46</sup>) and gas-phase (TS<sub>4</sub><sup>\*\*</sup>, C<sup>+0.03</sup>-O<sup>-0.44</sup>), as shown in Figure 4b. This observation was further asserted by the calculated dipole moment for TS<sub>4a</sub> (12.73 D) indicating towards a more polarized nature of the transition state, compared to TS<sub>4a</sub><sup>\*</sup> (7.22 D) and TS<sub>4</sub><sup>\*\*</sup> (6.1 D).



**Figure 4.** a) Reaction diagram for rDA reaction of 4HDMP in water, n-hexane and gas-phase. b) Mulliken charge analysis for the reactant (4a) and transition states in water (TS<sub>4a</sub>), n-hexane (TS<sub>4a</sub><sup>\*</sup>) and gas-phase (TS<sub>4a</sub><sup>\*\*</sup>).



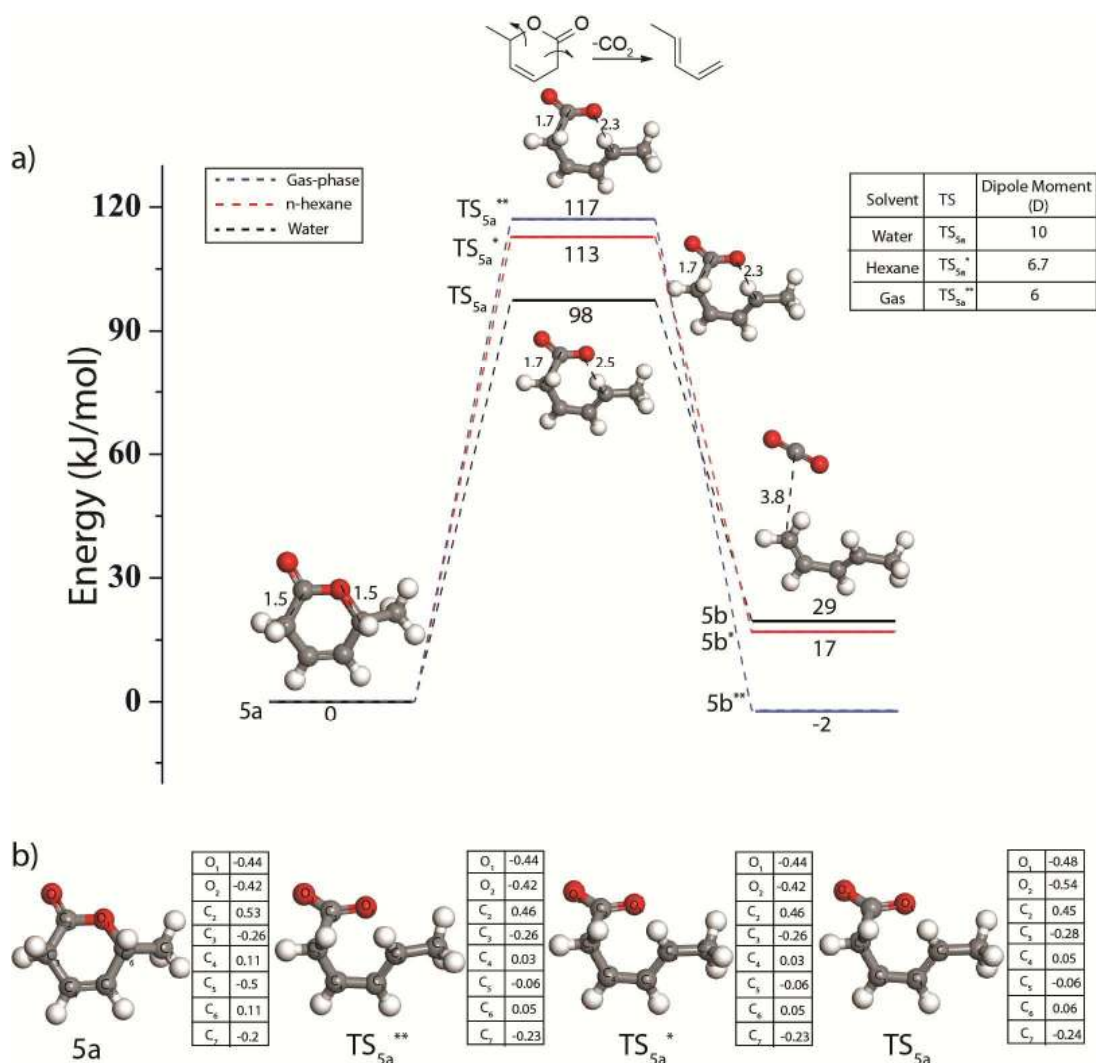
Due to the presence of an additional methyl group at C<sub>3</sub>, as compared to 5DHHMP, an increase in HOMO of the diene reduces the FMO gap to 0.1581 Hartree (Table 1). Interestingly, the reduced FMO gap did not lead to the reduction in activation energy in gas-phase, Table 1. This could possibly be explained by the steric hindrance offered by the methyl substituents. In order to separate the electronic and geometric effect of the methyl substituents, separate graphs were plotted for varying substituents at C<sub>3</sub>, C<sub>4</sub> and C<sub>6</sub>. Figure 5a shows a clear electronic effect of the electron donating –OH and –CH<sub>3</sub> substituents at the C<sub>4</sub> position, wherein the activation energy of the gas-phase rDA reaction scales linearly with the FMO gap. However, the presence of methyl group at C<sub>3</sub>, C<sub>4</sub> and C<sub>6</sub> shows a geometric effect which can be quantified separately on a linear scale with respect to the position and number as shown in Figure 5b and 5c. Clearly the two methyl groups at C<sub>6</sub> and C<sub>3</sub> in the 3,6-dimethyl-3,6-dihydro-2H-pyran-2-one (DDHP) structure led to maximum steric hindrance and therefore, a maximum value of activation energy (141 kJ/mol, Figure 5c) was calculated for the rDA reaction. Thus, both electronic and geometric (steric) effects of the substituents affect the activation energy of rDA reaction of substituted 2 pyrones. In order to compare reactivity due to these two effects, additional model pyrone molecule bearing amine (–NH<sub>2</sub>) functionality (4-NH<sub>2</sub>-DHHP) at C<sub>4</sub> position was studied. The activation barrier for the ring-opening of 4-NH<sub>2</sub>-DHHP was calculated to be 85 kJ/mol (Figure S2) which is lesser than DHHP (136 kJ/mole). Thereby, the electronic effect of substituent reduces activation barrier by 51 kJ/mol and steric effect lowers the activation barrier by 24 kJ/mol from 141 kJ/mol (DDHP) to 117 kJ/mol (4HMTHP). Therefore, the electronic effect can be considered to be more dominant than the steric effect.



**Figure 5.** Scaling of activation energies for rDA reaction of model molecules with respect to a) FMO gap (electronic effect) b) position of methyl (geometric effect) and c) number of methyl substituent (steric effect).

The electronic and geometric effect, of the methyl groups on the reactivity of partially saturated 2-pyrone molecules could be further explored by studying the rDA reaction on two additional molecules which are 6-methyl-3,6-dihydro-2H-pyran-2-one (4HMTHP) and 4,6,6-trimethyl-3,6-dihydro-2H-pyran-2-one (DTMP). Dumesic and co-workers have experimented and utilized these chemically synthesized molecules (4HMTHP and DTMP) for rDA reaction and have observed the trend in reactivity with respect to 5DHHMP to follow 5DHHMP>4HMTHP>DTMP. The reactivity of 5DHHMP with respect to the other two molecules was higher due to the presence of the hydroxyl at C<sub>4</sub> position, resulting into the formation of a stable zwitterionic intermediate in water. Interestingly, in the absence of the hydroxyl group at C<sub>4</sub>, the charged zwitterionic intermediate on ring-opening was not stable.

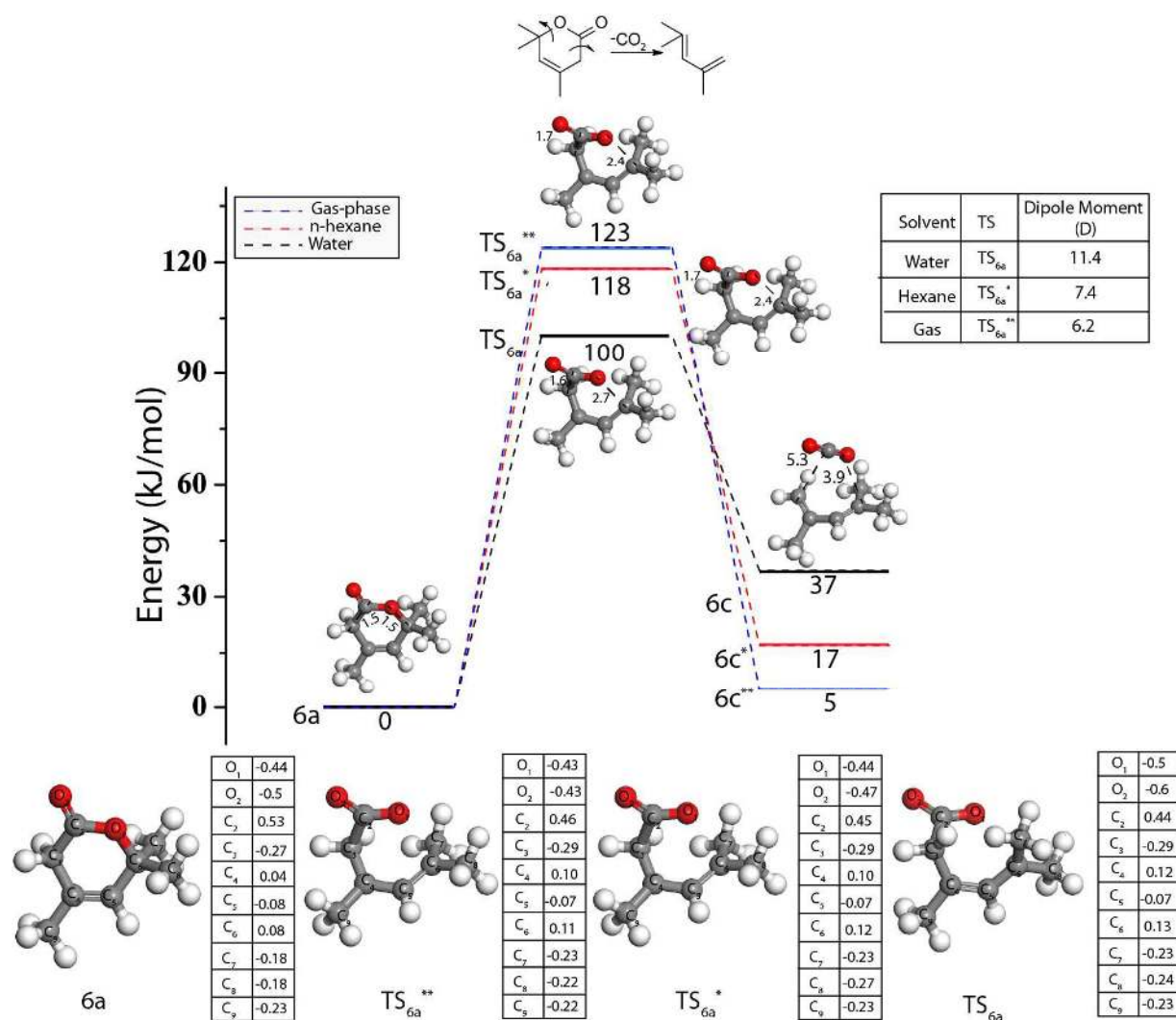
The electronic effect of the substituent at C<sub>4</sub> position was studied by performing DFT calculations on 4HMTHP as shown in Figure 6. Compared to 5DHHMP, the –OH substituent was not present in 4HMTHP. For the gas-phase calculation, the activation energy (117 kJ/mol) of rDA reaction (Figure 6, 5 to TS<sub>5</sub><sup>\*\*</sup>) of 4HMTHP was calculated to be higher than 5DHHMP, due to the increased FMO gap (0.177 hartree, Table 1). Unlike 5DHHMP, in aqueous phase, the rDA reaction of 4HMTHP was concerted with an activation barrier of 98 kJ/mole (Figure 6. 5a to TS<sub>5a</sub>), which is significantly reduced as compared to the gas-phase. However, in absence of any hydrogen bonding interactions with the solvent, activation barrier was calculated to be 113 kJ/mol (Figure 6. 5a to TS<sub>5a</sub><sup>\*</sup>) in n-hexane which is comparable to gas-phase estimations. The differences in the activation barrier in water compared to n-hexane and gas-phase could be attributed to greater charge polarization of the transition state in water (C<sup>+0.06</sup>-O<sup>-0.48</sup>) as compared to n-hexane (C<sup>+0.05</sup>-O<sup>-0.44</sup>) and gas-phase (C<sup>+0.05</sup>-O<sup>-0.44</sup>), Figure 6b. Consequently, the resultant transition state in water was calculated for maximum dipole moment (10 D) as compared to the one in n-hexane (6.7 D) and gas-phase (6 D), Figure 6. Ring-opening and decarboxylation of 4HMTHP produces 1,3-pentadiene which is used as a monomer for producing adhesives, plastics and resins<sup>44</sup>. Development of a process for the synthesis of 1,3-pentadiene from renewable feedstock is desirable and decarboxylation of biomass-derived sorbic acid have been tried to produce the same<sup>44</sup>. The rDA reaction of 4HMTHP could lead to an alternative route for the synthesis of 1,3-pentadiene where 4HMTHP has been shown to produce 1,3-pentadiene directly with a conversion of 22 % at 373 K<sup>11</sup>.



**Figure 6.** a) Reaction diagram for rDA reaction of 4HMTHP in water, n-hexane and gas-phase. b) Mulliken charge analysis for the reactant (5a) and transition states in water (TS<sub>5a</sub><sup>n</sup>), n-hexane (TS<sub>5a</sub><sup>\*</sup>) and gas-phase (TS<sub>5a</sub><sup>\*\*</sup>).

The geometric effect of the methyl substituent is elucidated in calculations of DTMP compared to 4HMTHP. The three electron donating methyl groups in DTMP led to a further reduction in the FMO gap to 0.1715 Ha as given in Table 1. On the contrary, the activation energy for rDA reaction was increased to 123 kJ/mol. This is likely due to the steric effect of the methyl substituents at C<sub>6</sub> and C<sub>4</sub> in DTMP. The activation energy for rDA reaction of di-methyl substituted 6,6-dimethyl-3,6-dihydro-2H-pyran-2-one is 126 kJ/mol (FMO gap = 0.1720) whereas the mono-methyl substituted 4HMTHP is 117 kJ/mol (FMO gap = 0.177). Likewise 4HMTHP, the ring-opening and decarboxylation of DTMP takes place via a concerted mechanism in water and n-hexane with an activation barrier of 100 kJ/mol (Figure 7 (6a to

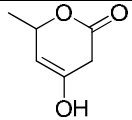
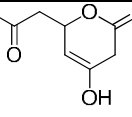
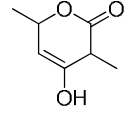
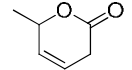
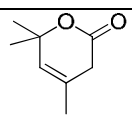
TS<sub>6a</sub>) and 118 kJ/mol (Figure 7 (6a to TS<sub>6a</sub><sup>\*</sup>)) respectively. The product 2,4-dimethylpenta-1,3-diene is used as a precursor for other chemicals<sup>45</sup>. The reaction energies were calculated to be 37 and 17 kJ/mol in water and n-hexane (Figure 5, 6c and 6c<sup>\*</sup>). Mulliken charge analysis on the transition state structures show that the charge separation and dipole moment in water (TS<sub>6a</sub>, C<sup>+0.13</sup>-O<sup>-0.5</sup>, 11.4 D) is significantly higher than n-hexane (TS<sub>6a</sub><sup>\*</sup>, C<sup>+0.12</sup>-O<sup>-0.44</sup>, 7.4 D) and gas-phase (TS<sub>6a</sub><sup>\*\*</sup>, C<sup>+0.11</sup>-O<sup>-0.43</sup>, 6.2 D), Figure 7b.



**Figure 7.** a) Reaction diagram for rDA reaction of DTMP in water, n-hexane and gas-phase. b) Mulliken charge analysis for the reactant (6a) and transition states in water (TS<sub>6a</sub>), n-hexane (TS<sub>6a</sub><sup>\*</sup>) and gas-phase (TS<sub>6a</sub><sup>\*\*</sup>).

The rate of uncatalyzed rDA reactions of all the molecules studied are observed to be dependent on solvent polarity. While reaction rates of ring-opening and decarboxylation of DHHMP were not measured experimentally, in general, the rates were observed to be accelerated in presence of water as compared to THF<sup>46</sup>. Assuming first order reaction, a theoretical comparison of reaction rate constants in polar and non-polar solvent can be made here. The rate constants of ring-opening and decarboxylation in water and n-hexane at 373 K of the five molecules studied are presented in Table 2. The rate constants were observed to be accelerated by over and above 1000 fold in water as compared to n-hexane. This is consistent with theoretical studies by Wijnen and Engberts, wherein the authors calculated the rate of rDA reaction of anthracenedione to proceed faster in water ( $k=359 \times 10^8 \text{ sec}^{-1}$ ) as compared to n-hexane ( $k=2.6 \times 10^8 \text{ sec}^{-1}$ ) and benzene ( $6.6 \times 10^8 \text{ sec}^{-1}$ )<sup>47</sup>. Similarly, the second order rate constant of DA reaction of cyclopentadiene and 5-methoxy-naphthoquinone were measured to be higher in water by 6000 fold than the rate constant in n-hexane<sup>48</sup>. In a solvent, the rates were affected by the type of substituent at C<sub>6</sub>, C<sub>3</sub> and C<sub>4</sub> following the same trend as observed for their calculated activation energies. Similar observations were made for the rDA reaction of 4H-1,2-Benzoxazines to generate o-Quinone methides in which reaction proceeded faster in polar solvents such as DMSO which was attributed to the stabilization of polarized TS structure. In addition, the reaction showed a clear effect on altering the position of the substituent on the benzene ring<sup>40</sup>.

**Table 2.** First-order rate constants calculated for the rDA reaction.

Compound	Rate constant in solvents	
	Water (1/sec)	n-hexane (1/sec)
 5DHHMP	158000	82.3
 4HOPP	175000	9.7
 4HDMP	5640	1.4
 4HMTHP	68.1	0.05
 DTMP	33.3	0.003

The extent of acceleration of rDA reaction rates could become more apparent on calculating the activation energies in a wide range of polar and non-polar solvents. Therefore, ring-opening of DTMP was studied in a range of polar (e.g. water, methanol, ethanol and dimethyl sulfoxide), non-polar (e.g. n-hexane) and slightly polar (e.g. chloroform) solvents. It was observed that the activation energy of rDA reaction was constant (~100 kJ/mol) in all the polar solvents studied, irrespective of their dielectric constant as shown in Figure 8a. However, the activation energy ( $E_a = 113$  kJ/mol) was slightly higher in case of chloroform likely due to lesser polarity (9.6 D). Similarly in n-hexane due to minimum polarity (7.4 D) the calculated activation energy was maximum compared to other solvents studied. Figure 8b shows the corresponding FMO gap of the product diene and  $\text{CO}_2$  for normal electron demand rDA reaction of DTMP for different



polar and non-polar solvents. On the same plot the dipole moment of the activated complex formed are shown. The FMO gap for polar solvents (e.g. methanol, ethanol, DMSO and water) is of similar value (0.18 Ha), which is higher than n-hexane (0.1720 Ha), chloroform (0.1776 Ha) and gas-phase (0.1715 Ha). Interestingly, an increased FMO gap in polar solvents did not lead to an increase in the activation energies of the rDA reaction. Instead, reduced value of activation barriers were calculated in polar solvents compared to non-polar and gas-phase reactions, which is likely due to the stabilization of the activated complexes formed during the course of reaction. The increased polarization of transition states in polar solvents is reflected in their calculated dipole moments which are significantly higher than the respective structures formed in non polar and gas-phase calculations, Figure 8b. Thus, the FMO theory does not directly follow in case of solvents and a separate descriptor to explain the reactivity trends in solvents needs to be explored. This shall be discussed in a separate communication.

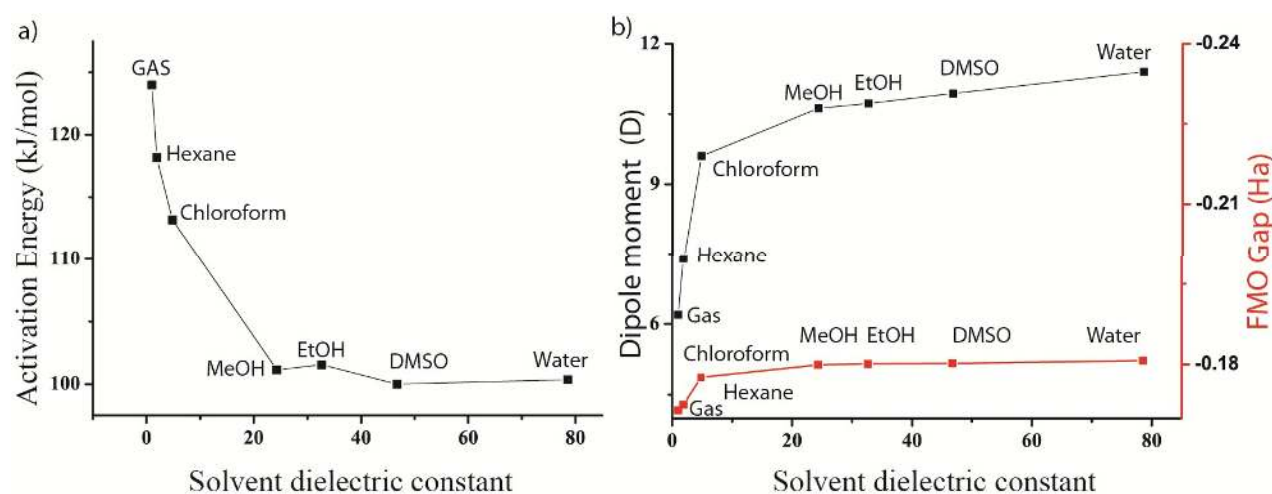


**Figure 8.** Variation of a) activation energy b) dipole moment and FMO gap of DTMP with respect to solvent dielectric constant for the rDA reaction.

Models to predict reactivity trends with respect to the energetics of the reaction, has been a topic of great interest<sup>49</sup>. For example, in a study on uncatalyzed 1,4 hydrogenation reaction of polycyclic aromatic hydrocarbons (PAHs), the reaction energies were calculated to linearly scale with the activation energies following the BEP principle<sup>50</sup>. Interestingly, the DFT calculated transition state and reaction energies of uncatalyzed rDA reaction of the studied molecules is effectively described by BEP relationship. The plotted linear trends are shown in Figure 9. The trend was observed in gas-phase as well as water and n-hexane. While the trends

are considered linear ( $R^2 > 0.75$ ) within the errors of DFT ( $< 10\%$ ), the proportionality constants differ and BEP is more pronounced in water as compared to n-hexane. In general, the reaction energy values are higher in water as compared to n-hexane and gas-phase, likely due to the differential stabilization of reactant versus product by hydrogen bonding interactions. For the same reaction, the activation energies calculated are lowest for water as compared to n-hexane and gas-phase.

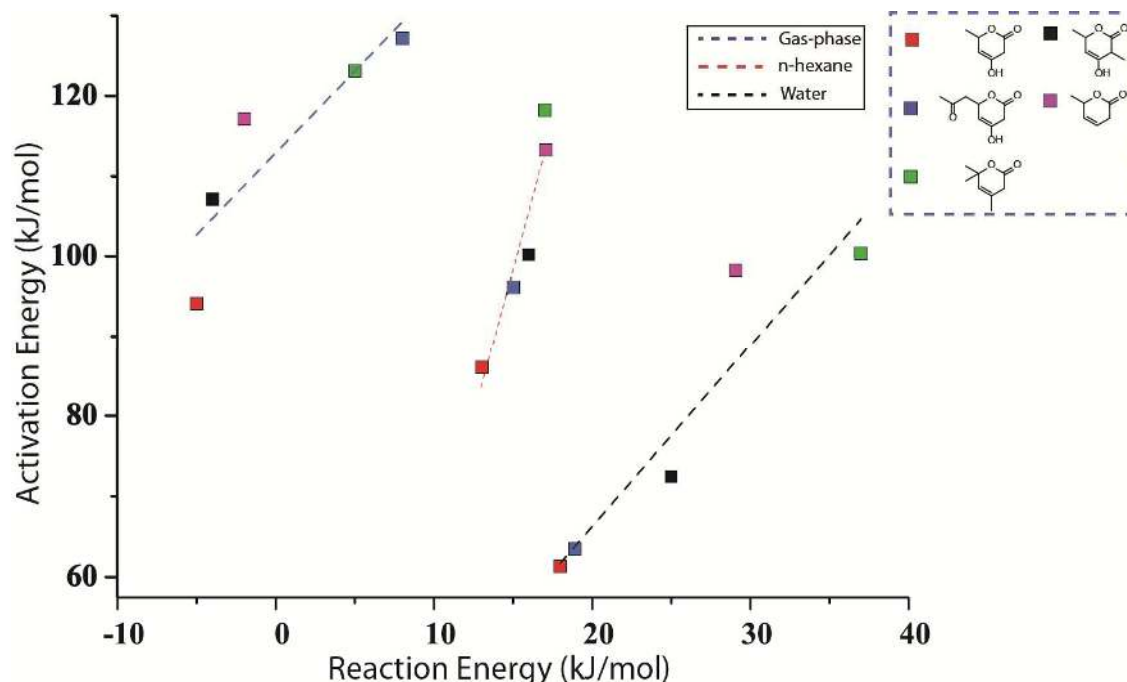


**Figure 9.** BEP relationship for the calculated activation barrier versus reaction energies in gas-phase, n-hexane and water.

In presence of a Brønsted acid catalyst such as Amberlyst-70, the ring-opening barrier for DHHMP was significantly reduced and measured to be 18 kJ/mol<sup>11</sup>. This was explained in the previous study by an increase in the number of active acidic sites, enabling faster KET reaction. However, a quick observation of the reported reaction diagram reveals that the KET step is in an equilibrium. Thus an alternative mechanism for acid catalyzed rDA reaction is hypothesized in this study. In this route, a proton is expected to attack the carbonyl oxygen forming an oxocarbenium ion. In a separate work on acid-catalyzed ring-opening of lactones, Gupta *et. al.* have hypothesized the formation of stable oxocarbenium intermediates which play an important role in ascertaining the rates of ring-opening<sup>51</sup>. The oxocarbenium ion thus formed undergo ring-opening with a relatively lower activation barrier of 15 kJ/mol (Figure 9), which is comparable to

the experimentally measured value. The acid-catalyzed rDA reaction proceeds in three steps as shown in Figure 10 wherein the barrier for decarboxylation step is of similar value (6 kJ/mol) as of uncatalyzed reaction. The lowering of activation barrier led to an overall enhancement of the rate of acid catalyzed rDA reaction as compared to uncatalyzed reaction. Similar reduction in the activation energies are reported for acid catalyzed DA reaction of the cycloadditions of 2,5-dimethylfuran and maleic anhydride compared to the uncatalyzed reaction. A proton in the presence of a Brønsted acid binds to the carbonyl group in maleic anhydride and reduces the activation barrier for the cycloaddition step<sup>42</sup>. Experiments and theoretical studies by Chia *et al.* on C-O hydrogenolysis reactions of cyclic ethers have shown a clear trend in reactivity with respect to the relative stabilization of resulting oxocarbenium structures<sup>52</sup>. Similar experiments may be performed for acid catalyzed reaction of 2-pyrone molecules, measuring the rate of ring-opening and decarboxylation which can be further correlated to the stability of oxocarbenium ion structures. With the available experimental results on catalytic transformation of 2-pyrones and mechanistic insights on rDA reaction developed in this study, novel processes may be designed which will pave the way for producing fuels and chemicals from biomass.

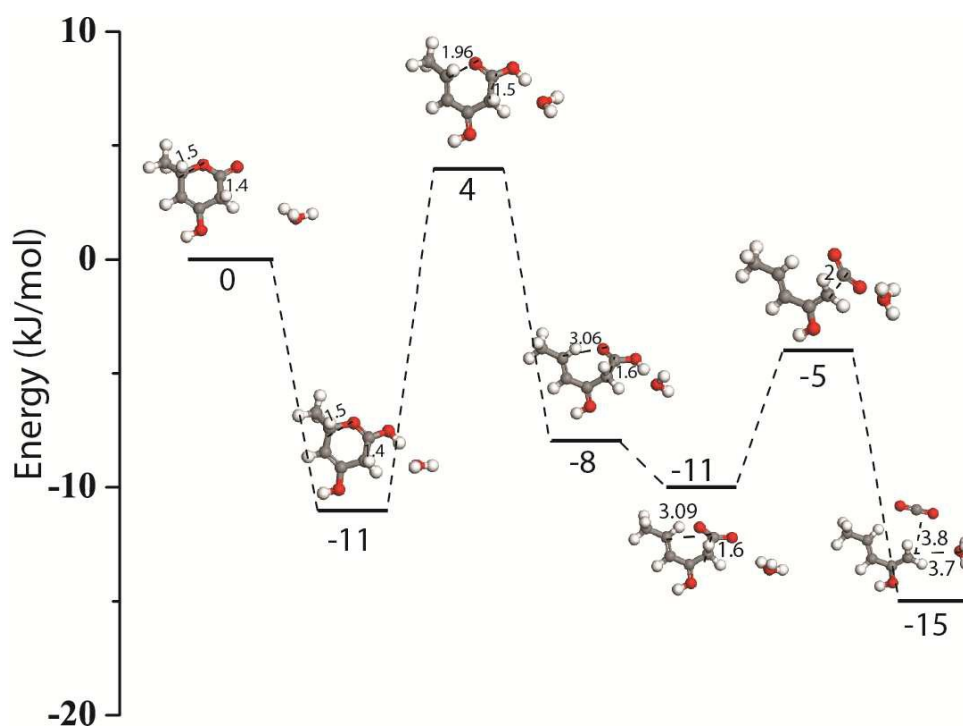


**Figure 10.** DFT calculated energy diagram for Brønsted acid catalyzed rDA reaction of 5DHHMP in water.

#### 4. CONCLUSIONS

The presence of a double bond at C<sub>4</sub>=C<sub>5</sub> position in partially saturated 2-pyrone led to ring-opening and decarboxylation via rDA reaction. DFT calculations predicted that the nature, number and position of the substituents on the molecule affect the activation barrier of the rDA reaction. In general, electron donating group on the product diene reduces the barrier by reducing the FMO gap, whereas electron withdrawing group increases the barrier. The number and position of a specific substituent group on the diene were calculated to cause a separate geometric effect by introducing a steric effect. In addition to electronic and geometric (steric) effects, distortion energy (energy required to distort the reactants from their initial geometries to the transition state geometry) are also suggested to be a dominant factor to explain reactivity trends in Diels Alder reaction<sup>53,54</sup>. In order to find the most dominant and universal descriptor between the electronic effect (FMO gap) and distortion energy, a detail study is essential which will be undertaken as a future work to develop insights into these factors for explaining reactivity of rDA reaction. The hydroxyl group at C<sub>4</sub> position helped in deciding the nature of rDA (concerted or a two-step mechanism) reaction in water via the formation of a stable zwitterionic intermediate. Nevertheless, for all cases, the reaction was calculated to be concerted in n-hexane and gas-phase. While, the electronic effect was linearly correlated to the FMO gap of products in gas-phase, the theory did not hold true in water and n-hexane. In a specific solvent, the rDA reaction of the molecules was observed to follow a BEP relationship. Under acidic conditions, a three-step rDA was suggested to occur via the formation of a stable oxocarbenium ion intermediate. The results thus highlight the reactivity trend of partially saturated biomass-derived 2-pyrone molecules for rDA reaction by establishing the role of solvent and substituents.

#### ACKNOWLEDGEMENTS

The authors would like to acknowledge the help provided by Dr. Manish Agarwal in the Computer Service Center at IIT Delhi in setting up the calculations. We acknowledge the financial support from the Department of Biotechnology (BT/COE/34/SP15097/2015), Government of India to carry out this work. SG thanks IIT Delhi for providing research fellowship.

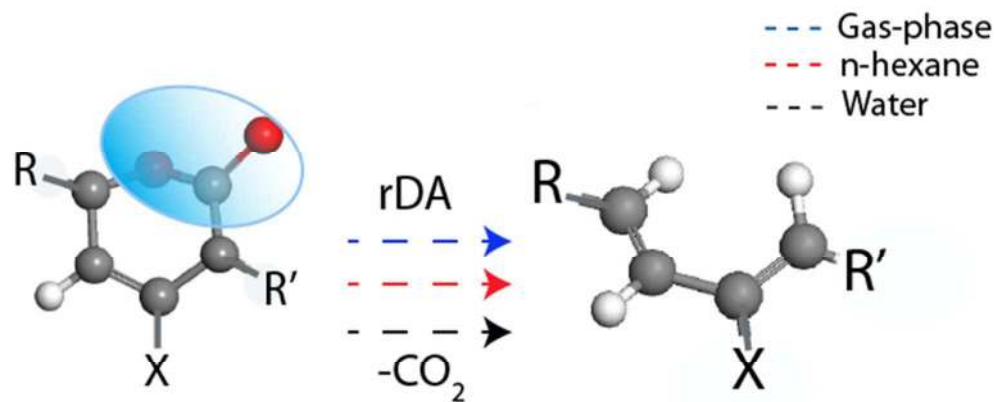
## REFERENCES

- 1 M. I. Alam, S. De, B. Singh, B. Saha and M. M. Abu-Omar, *Appl. Catal. A Gen.*, 2014, **486**, 42–48.
- 2 M. J. Climent, A. Corma and S. Iborra, *Green Chem.*, 2014, **16**, 516–547.
- 3 T. J. Schwartz, B. J. O. Neill, B. H. Shanks and J. A. Dumesic, *ACS Catal.*, 2014, **4**, 2060–2069.
- 4 T. J. Schwartz, B. H. Shanks and J. A. Dumesic, *Curr. Opin. Biotechnol.*, 2016, **38**, 54–62.
- 5 K. P. Somers, J. M. Simmie, W. K. Metcalfe and H. J. Curran, *Phys. Chem. Chem. Phys.*, 2014, **16**, 5349–5367.
- 6 C. Wen, E. Barrow, J. Hatrick-Simpers and J. Lauterbach, *Phys. Chem. Chem. Phys.*, 2014, **16**, 3047–3054.
- 7 J. Guan, G. Peng, Q. Cao and X. Mu, *J. Phys. Chem. C*, 2014, **118**, 25555–25566.
- 8 C.-T. Wu, J. Qu, J. Elliott, K. M. K. Yu and S. C. E. Tsang, *Phys. Chem. Chem. Phys.*, 2013, **15**, 9043–9050.
- 9 P. Kostestkyy, J. P. Maheswari and G. Mpourmpakis, *J. Phys. Chem. C*, 2015, **119**, 16139–16147.
- 10 M. Chia, T. J. Schwartz, B. H. Shanks and J. A. Dumesic, *Green Chem.*, 2012, **14**, 1850–1853.
- 11 M. Chia, M. A. Haider, G. Pollock, G. A. Kraus, M. Neurock and J. A. Dumesic, *J. Am. Chem. Soc.*, 2013, **135**, 5699–5708.
- 12 J. Q. Bond, D. M. Alonso, D. Wang, R. M. West and J. A. Dumesic, *Science*, 2010, **327**, 1110–4.
- 13 S. Eckermann, G. Schroder, J. Schmidt, D. Strack, R. A. Edrada, Y. Helaroutta, P. Elomaa, M. Kotilainen, I. Kilpelaines and J. Schroder, *Nature*, 1998, **396**, 387–390.
- 14 S. K. Bardhan, S. Gupta, M. E. Gorman and M. A. Haider, *Renew. Sustain. Energy Rev.*, 2015, **51**, 506–520.
- 15 M. I. Alam, S. Gupta, E. Ahmad and M. A. Haider, in *Sustainable Catalytic Processes*, 2015, pp. 157–177.
- 16 J. Cardenas and N. A. Da Silva, *Metab. Eng.*, 2014, **25**, 194–203.
- 17 A. Goel and V. J. Ram, *Tetrahedron*, 2009, **65**, 7865–7913.
- 18 N. Funa, Y. Ohnishi, Y. Ebizuka and S. Horinouchi, *J. Biol. Chem.*, 2002, **277**, 4628–35.
- 19 R. Bentley and P. M. Zwitkowitz, *J. Am. Chem. Soc.*, 1967, **89**, 1967.
- 20 J. M. Dickinson, *Nat. Prod. Rep.*, 1993, **10**, 71–98.
- 21 X. Yang and Y. Xue, *Phys. Chem. Chem. Phys.*, 2013, **15**, 11846–55.
- 22 G. K. van der Wel, J. W. Wijnen and J. B. F. N. Engberts, *J. Org. Chem.*, 1996, **61**, 9001–9005.

- 23 S. Wilsey, K. N. Houk and A. H. Zewail, *J. Am. Chem. Soc.*, 1999, **121**, 5772–5786.
- 24 A. L. W. Demuynck, P. Levecque, A. Kidane, D. W. Gammon, E. Sickle, P. A. Jacobs, D. E. De Vos and B. F. Sels, *Adv. Synth. Catal.*, 2010, **352**, 3419–3430.
- 25 O. Henri-rousseau and F. Texier, *J. Chem. Educ.*, 1978, **55**, 437–441.
- 26 D. H. Ess, G. O. Jones and K. N. Houk, *Adv. Synth. Catal.*, 2006, **348**, 2337–2361.
- 27 Y. Chung, B. F. Duerr, T. A. Mckelvey, P. Nanjappan and A. W. Czarnik, *J. Org. Chem.*, 1989, **54**, 1018–1032.
- 28 J. N. Bronsted, *Chem. Rev.*, 1928, **5**, 231–338.
- 29 M. G. Evans and M. Polanyi, *Trans. Faraday Soc.*, 1937, **34**, 11–24.
- 30 B. Delley, *J. Chem. Phys.*, 1990, **92**, 508.
- 31 L. Wang and M. P. Teter, *Phys. Rev. B*, 1992, **45**, 13244–13249.
- 32 A. Klamt, V. Jonas, T. Bu, J. C. W. Lohrenz, B. Ag and D.- Le V, *J. Phys. Chem. A*, 1998, **5639**, 5074–5085.
- 33 T. A. Halgren and W. N. Lipscomb, *Chem. Phys. Lett.*, 1977, **49**, 225–232.
- 34 R. S. Mulliken, *J. Chem. Phys.*, 1955, **23**, 1833.
- 35 K. Shin, D. H. Kim, S. C. Yeo and H. M. Lee, *Catal. Today*, 2012, **185**, 94–98.
- 36 R. Liu, W. Shen, J. Zhang and M. Li, *Appl. Surf. Sci.*, 2008, **254**, 5706–5710.
- 37 J. Chandrasekhar, S. Shariffskul and W. L. Jorgensen, *J. Phys. Chem. B*, 2002, **106**, 8078–8085.
- 38 E. W. Diau, S. De Feyter and A. H. Zewail, *Chem. Phys. Lett.*, 1999, **304**, 134–144.
- 39 A. Meijer, S. Otto and J. B. F. N. Engberts, *J. Org. Chem.*, 1998, **63**, 8989–8994.
- 40 H. Sugimoto, S. Nakamura and T. Ohwada, *J. Org. Chem.*, 2007, **72**, 10088–10095.
- 41 V. M, C. U, V. P.A. and G. R, *J. inorg. nucl. Chem.*, 1976, **38**, 1455–1459.
- 42 T. Salavati-Fard, S. Caratzoulas and D. J. Doren, *J. Phys. Chem. A*, 2015, **119**, 9834–9843.
- 43 G. A. Burdock, *Fenaroli's handbook of flavor ingredients*, CRC Press Boca Raton, FL, Sixth Edit., 2010.
- 44 US 12/943,433, 2012, 1, 1–9.
- 45 N. I. Shuikin, T. I. Naryshkina and Z. A. Rashchupkina, *Pet. Chem. U.S.S.R.*, 1963, **2**, 16–20.
- 46 J. W. Wijnen and J. B. F. N. Engberts, *Liebigs Ann.*, 1997, **1997**, 1085–1088.
- 47 J. W. Wijnen and J. J. B. F. N. Engberts, *J. Org. Chem.*, 1997, **62**, 2039–2044.
- 48 B. W. Blokzijl and J. B. F. N. Engberts, *Angew. Chem. Int. Ed. Engl.*, 1993, **32**, 1545–1579.
- 49 A. Vojvodic, F. Abild-Pedersen and F. Illas, *J. Phys. Chem. C*, 2013, **117**, 4168–4171.
- 50 G. Zhong, B. Chan and L. Radom, *J. Mol. Struct. THEOCHEM*, 2007, **811**, 13–17.



- 51 S. Gupta, R. Arora, N. Sinha, I. Alam and M. A. Haider, *RSC Adv.*, 2016, **6**, 12932–12942.
- 52 M. Chia, Y. J. Pag, D. Hibbitts, Q. Tan, H. N. Pham, A. K. Datye, M. Neurock, R. J. Davis and J. A. Dumesic, *J. Am. Chem. Soc.*, 2011, **133**, 12675–12689.
- 53 A. E. Hayden and K. N. Houk, *J. Am. Chem. Soc.*, 2009, 4084–4089.
- 54 B. J. Levandowski and K. N. Houk, *J. Org. Chem.*, 2015, **80**, 3530–3537.



108x79mm (150 x 150 DPI)